


# An operationally broadened alkaline water electrolyser enabled by highly stable poly(oxindole biphenylene) ion-solvating membranes

Received: 13 October 2022

Accepted: 15 December 2023

Published online: 15 January 2024

 Check for updates

Xu Hu<sup>1,2</sup>, Bin Hu<sup>1,2</sup>, Chengyuan Niu<sup>1</sup>, Jin Yao<sup>3</sup>, Min Liu<sup>1,2</sup>, Huabing Tao<sup>4</sup>, Yingda Huang<sup>1</sup>, Shuanyan Kang<sup>1</sup>, Kang Geng<sup>1</sup>✉ & Nanwen Li<sup>1,2</sup>✉

Ion-solvating membranes (ISMs) are an alternative to proton-exchange and anion-exchange membranes for use in water electrolysers. ISMs do not have fixed ionic groups in their structure but instead gain their ionic conductivity through the uptake of liquid electrolyte. Although in principle they could offer improved stability over anion-exchange membranes due to the absence of easily degradable anion-exchange groups, stability gains have been modest. Here we report poly(oxindole biphenylene)-based ISMs with highly stable oxindole/KOH complex ion pairs for use in water electrolysers. These ISMs exhibit promising alkaline stability at 80 °C with a negligible conductivity decay over more than 15,000 h and, thus, allow durable alkaline electrolysis over 2,500 h, even at elevated temperatures and high operating voltages of 2.3 V. Moreover, they show ultralow gas permeation and, thus, low transient response times (<1 s). They allow the use of non-precious-metal catalysts (Ni and Ni/Fe) and can be operated over a broad temperature range (−35 to 120 °C).

Water electrolysis can be used to store electricity from renewable energy sources in chemical bonds in the form of high-purity hydrogen<sup>1</sup>. Traditional alkaline electrolysers with a circulating 30–40 wt% KOH and a porous diaphragm have the primary advantage of allowing the utilization of inexpensive non-platinum-metal (PGM) catalysts (such as Ni foam) under alkaline conditions<sup>2</sup> and even at elevated temperature<sup>3,4</sup>. However, the porous diaphragms in alkaline water electrolysers (AWEs) result in high gas permeation and blow-out of the electrolyte. As a result, these systems are not effective at elevated current densities (<500 mA cm<sup>−2</sup>) and display a high transient response time to maintain a balanced pressure, making them unsuitable for renewable energy source applications<sup>2,5</sup>.

Thus, polymeric electrolyte membranes (such as proton-exchange membranes (PEMs) and anion-exchange membranes (AEMs)) have been

developed to replace porous diaphragms with liquid electrolytes<sup>6,7</sup>. In this case, the dense PEMs and AEMs have excellent ability as a gas barrier. Thus, the use of dense membranes in water electrolysis allows the design of a compact system with durable and resistant structural properties at high differential pressures and rapid transient response times that is adaptable to the fluctuation of renewable energy sources, such as wind and solar energy. Although PEM electrolysers have advantages due to the high stability and durability of perfluorosulfonic acid membranes, they have the disadvantage of high capital cost due to the need for high loadings of platinum and iridium catalysts (IrO<sub>2</sub>) as well as precious-metal-coated titanium porous transport layers and bipolar plates<sup>5,7</sup>. In contrast, an AEM electrolyser based on a polymer with fixed cationic side groups<sup>8</sup> has the advantages of using a low-cost PGM-free

<sup>1</sup>State Key Laboratory of Coal Conversion, Institute of Coal Chemistry, Chinese Academy of Sciences, Taiyuan, China. <sup>2</sup>Center of Materials Science and Optoelectronics Engineering, University of Chinese Academy of Sciences, Beijing, China. <sup>3</sup>Ningbo Sino-Tech Hydrogen Membrane Technology Co., Ltd, Ningbo, China. <sup>4</sup>State Key Laboratory for Physical Chemistry of Solid Surfaces, Collaborative Innovation Center of Chemistry for Energy Materials, and College of Chemistry and Chemical Engineering, Xiamen University, Xiamen, China. ✉e-mail: [gengkang@sxicc.ac.cn](mailto:gengkang@sxicc.ac.cn); [linanwen@sxicc.ac.cn](mailto:linanwen@sxicc.ac.cn)

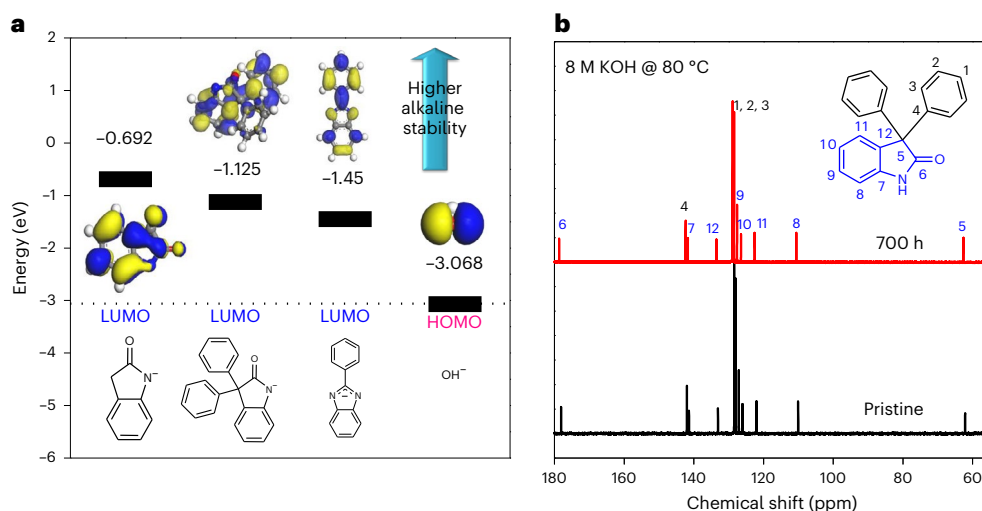


**Fig. 1 | DFT calculation and alkaline stability of model compounds.** **a**, Calculated LUMO energies and isosurfaces of deprotonated model compounds and HOMO energy of  $\text{OH}^-$ . The higher the LUMO energy, the higher the alkaline stability of the molecule. **b**, Alkaline stability from  $^{13}\text{C}$  NMR of 3,3-diphenylhydroxyindole in 8 M KOH at 80 °C.

catalyst as well as low gas permeation. However, the insufficient alkaline stability of AEMs (<5,000 h) and device durability at elevated temperatures above 60 °C due to  $\text{S}_{\text{N}}2$  substitution<sup>9</sup> and Hoffman elimination<sup>6</sup> of fixed cationic groups and free radical attack<sup>10</sup> in an electrochemical environment remain crucial challenges for AWE applications.

Thus, an operationally flexible polymer electrolyte membrane with high alkaline and device stability at elevated temperatures ( $\geq 80$  °C), and good ion conduction is desired to bridge the gap in these water electrolysis technologies<sup>2</sup>. When a polymer is used as a membrane under alkaline water electrolysis, the fixed cationic groups may substantially limit the stability. For example, alkaline-doped polybenzimidazole (PBI)<sup>11</sup> and  $\text{ZrO}_2/\text{PSf}$  membranes<sup>12</sup>, which do not have fixed ionic groups, are much more stable than the sulfonated and quaternized hydrocarbon polymers. Owing to the highly ionic conduction of liquid KOH electrolytes, fixed cationic groups are not essential for intrinsic ion conduction in alkaline membranes. However, in this case, functional groups are needed in the polymer so that a homogeneous ternary polymer/water/KOH electrolyte system forms when imbibed with KOH.

Ion-solvating membranes (ISMs)<sup>12,13</sup> utilize the uptake and presence of an aqueous alkaline electrolyte to achieve ionic conductivity. Thus, a weak-base polymer, such as PBI, when doped with KOH was first demonstrated as an ISM (ref. 14). This system exhibits promising alkaline stability for up to 2,000–5,000 h, which is much longer than that of an AEM with a fixed cationic group<sup>15</sup>. An assembled alkaline electrolyser with optimized RANEY-type electrodes achieved an impressive performance of 1.7 A  $\text{cm}^{-2}$  at 1.8 V and a wide operating current density<sup>12</sup>. Nevertheless, notable degradation by the ring-opening of deprotonated benzimidazole moieties in the cell potential and eventual cell failure were also observed during long-term tests when the operating temperature was more than 60 °C (refs. 12,15,16). Moreover, the fluctuation of renewable energy and its distribution in cold regions, such as north-western China, necessitates a readily repeatable low-temperature electrolyser start-up process if additional heating is to be avoided. However, the pure water in a PEM water electrolyser or the low concentration of aqueous KOH in an AEM water electrolyser may freeze under such conditions, and thus, the electrolyser may fail during a cold start-up without an additional heating system<sup>17,18</sup>. Thus, realizing stable operation over a broad range of temperatures in an alkaline environment is a critical challenge for water electrolyzers with a polymer electrolyte membrane.

In this work, we demonstrate that ISM AWEs based on highly stable oxindole/KOH complex ion pairs in poly(oxindole biphenylene) (POBP), which have been prepared by superacid-catalysed polymerization<sup>19</sup> and have previously been used for gas separation<sup>20</sup>, AEMs<sup>21</sup> and ultrafiltration<sup>22</sup>, can avoid the limitations of traditional water electrolysis based on AWEs, PEMs or AEMs, thus enabling operations under a wide range of conditions that are not accessible with existing electrolysis technology. This ISM can conduct ions through stable oxindole/KOH complex ion pairs and enable AWE operation using a non-precious-metal catalyst of Ni foam or Ni/Fe. It has long durability over a broad temperature range from –35 to 120 °C and ultralow gas permeation and thus transient response times (<1 s).

### LUMO energy and alkaline stability of deprotonated anion

The operational durability of ISMs in AWEs at an elevated temperature is dictated by the lowest unoccupied molecular orbital (LUMO) energy of the deprotonated base moieties in water. The highest occupied molecular orbital (HOMO) energy of  $\text{OH}^-$  (in water), as determined with density functional theory (DFT) calculations<sup>23</sup>, is –3.068 eV, which is lower than the LUMO energy of deprotonated benzimidazole anions. Thus, nucleophilic attacks of  $\text{OH}^-$  are limited by the LUMO energy of deprotonated benzimidazole anions. As a result, a higher LUMO energy will make it more difficult for deprotonated benzimidazole anions to be attacked by  $\text{OH}^-$  anions. As shown in Fig. 1a, deprotonated benzimidazole has a LUMO energy of –1.450 eV, which is 1.618 eV higher than the HOMO energy of  $\text{OH}^-$ . However, the LUMO energies of deprotonated oxindole and 3,3-diphenylhydroxindole in water were calculated to be –0.692 and –1.125 eV, respectively. These values are greater than those of the deprotonated benzimidazole anion, indicating the difficulty of attack by  $\text{OH}^-$  and, thus, the potentially high alkaline stability. To further confirm the alkaline stability of the deprotonated oxindole anion, the model compound 3,3-diphenyloxindole was designed and synthesized by superacid-catalysed reactions<sup>24</sup>. Subsequently, the alkaline stability of the model compound was determined in 8 M KOH at 80 °C. As expected, no obvious degradation was observed after 700 h of testing, as determined by  $^{13}\text{C}$  nuclear magnetic resonance (NMR) and  $^1\text{H}$  NMR (Fig. 1b and Supplementary Fig. 1). In contrast, benzimidazole degraded due to the ring-opening reaction of imidazole groups after only 700 h under the same testing conditions (Supplementary Figs. 2 and 3).

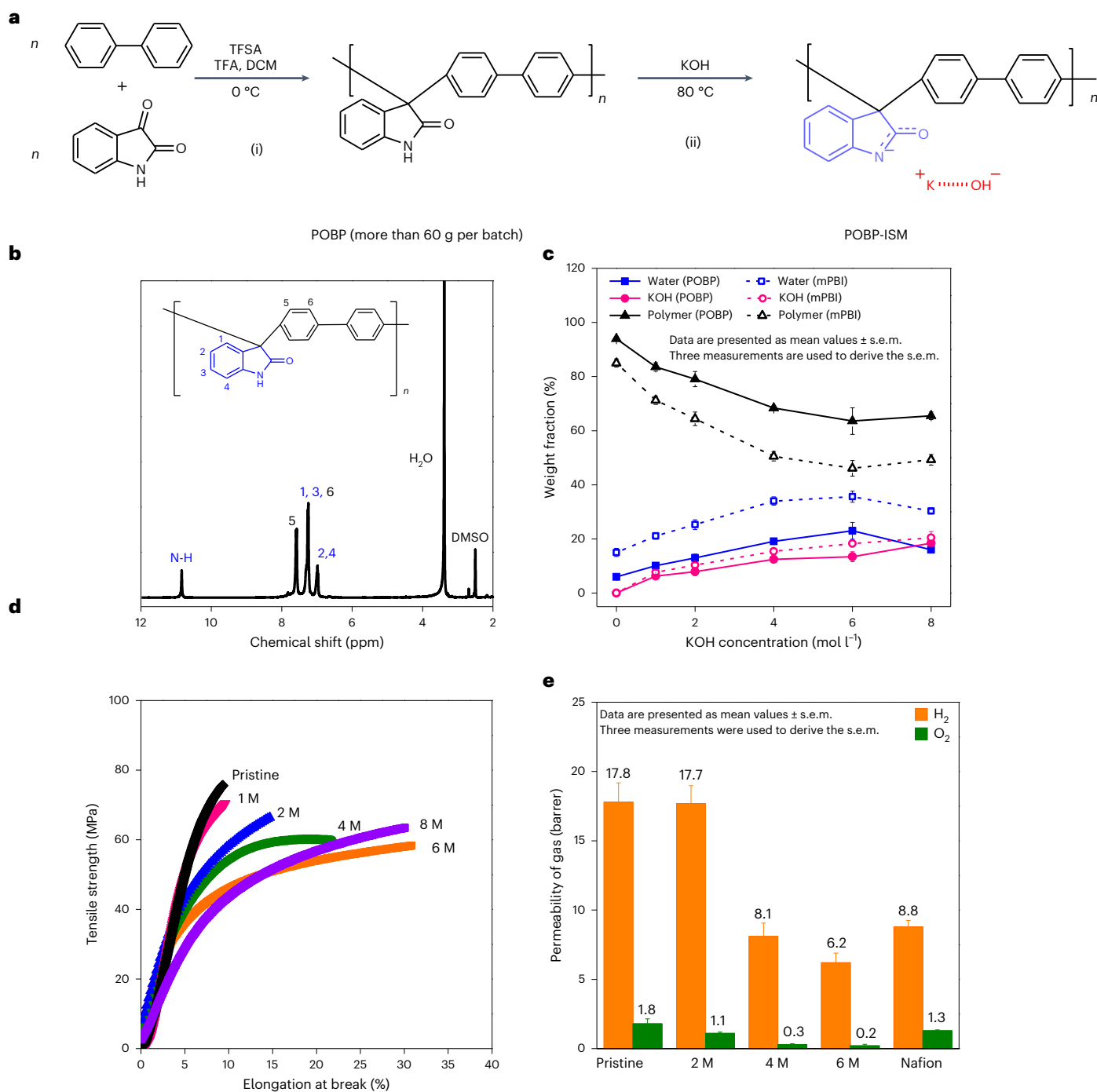


**Fig. 2 | Preparation and characterization of POBP-ISM. a**, Synthesis of POBP-ISM. **b**, <sup>1</sup>H NMR spectra of a POBP membrane. **c**, Composition with respect to the total ISM (POBP/H<sub>2</sub>O/KOH) weight of the wet form. **d**, Mechanical properties of POBP-ISM membranes as a function of KOH concentration. **e**, Gas permeability of

POBP-ISM membranes as a function of KOH concentration in the dry state. Error bars in **c** and **e** were generated from the standard error of the mean (s.e.m.) derived from three measurements.

## Synthesis, membrane preparation and characterization

Subsequently, as shown in Fig. 2a, oxindole was successfully introduced into the aryl-ether-free polymer by superacid-catalysed polymerization of biphenyl and isatin to produce POBP (ref. 25). A <sup>1</sup>H NMR analysis confirmed the polymer structure<sup>19</sup> (Fig. 2b). Despite the rigid polymer backbone of POBP, as confirmed by the high glass transition temperature (*T<sub>g</sub>*) of over 500 °C (Supplementary Fig. 4), high molecular weights were obtained (MW > 60,000 Da), and the polymer displayed excellent solubility in common solvents, such as dimethyl sulfoxide

(DMSO), *N*-methyl-2-pyrrolidone, *N,N*-dimethylformamide (DMF) and *N,N*-dimethylacetamide (Supplementary Table 1). An intrinsic viscosity in DMF of 2.20 dl g<sup>-1</sup> (Supplementary Table 2) was achieved, which satisfies the requirement for a thin, transparent membrane with a large area (Fig. 2b).

A tough, flexible and transparent POBP membrane was obtained by casting. Subsequently, the POBP membrane was submerged in aqueous KOH to obtain an ion-conductive ISM (Fig. 2a). The composition of the ternary electrolyte system (POBP/H<sub>2</sub>O/KOH) of the ISM was used to evaluate the concentration of KOH in the ISM, as this has an important

influence on the ionic conductivity. Generally, a high concentration of KOH electrolyte leads to a high KOH concentration in the ISM. Thus, as shown in Fig. 2c, the concentration of KOH in the POBP/H<sub>2</sub>O/KOH system increased from 6.31% to 18.46% when the KOH was increased from 1 M to 8 M. However, these values are slightly lower than those of the membrane-based polybenzimidazole (mPBI), which ranged from 7.66 to 20.43%. Because of the similar ion-pair interaction between a deprotonated anion and a K ion (118.23 kcal mol<sup>-1</sup> for deprotonated oxindole and 108.24 kcal mol<sup>-1</sup> for benzimidazolium, respectively), as confirmed by the DFT calculation (Supplementary Fig. 5), and, thus, the similar pK<sub>a</sub> values<sup>26,27</sup>, it is believed that the relatively low KOH absorption of the POBP membrane is attributed to its lower concentration of oxindole functional groups than that of the imidazole groups in mPBI. In addition to the KOH concentration in the membrane, the water concentration also plays a key role in ionic conductivity<sup>13</sup>. The water uptake of the membrane increased from 10.13% to 23%, whereas that of KOH increased from 6.31% to 13.45% when the KOH electrolyte was increased from 1 M to 6 M, respectively (Fig. 2c). The water uptake of the membrane decreased when the concentration of KOH electrolyte increased to 8 M despite its increased KOH concentration. Thus, the POBP membrane doped with 6 M KOH had the highest wettability (Supplementary Fig. 6). It is believed that excessive KOH concentration will result in a decrease in the amount of water held in the polymer matrix due to the concentrating effect of the polymer phase with respect to water in the higher KOH concentration regime and extensive crystallization of the polymer matrix<sup>13</sup>, as evidenced by the gravimetric (Fig. 2c) and X-ray diffraction (XRD) results. The results for the composition and hydrophilicity of the membranes initially suggested that the optimum concentration of KOH for the POBP-ISMs is 6 M, which was fully verified by the subsequent conductivity analysis. Further information on the swelling behaviour and XRD of the KOH-doped POBP membrane is given in Supplementary Note 1 (including Supplementary Figs. 7–9).

<sup>1</sup>H NMR, IR spectroscopy and X-ray photoelectron spectroscopy (XPS) were conducted to confirm the chemical structures of KOH-doped POBP-ISMs. As shown in Supplementary Fig. 10, the proton peak for NH in the oxindole in KOH-doped POBP-ISMs completely disappears after treatment with KOH, even at a low concentration of 1 M, indicating successful deprotonation. Moreover, the chemical shifting of benzene peaks to higher levels in the <sup>1</sup>H NMR results (Supplementary Fig. 10) further suggests the successful formation of anions, which act as electron-donating groups for the benzene ring. Obviously, the chemical shifting of benzene peaks increases with an increasing concentration of KOH. We assume that the high KOH concentration results in a strong interaction between deprotonated oxindole and K ions<sup>28</sup>. Moreover, DFT calculations show that both the N and O atoms interact with K ions. We assume that the N anion in oxindole tends to form a conjugated anion by rearrangement and equilibrium<sup>26,27</sup> (Fig. 2a and Supplementary Figs. 5 and 11). Thus, the stretching vibration bands of the C=O in oxindole at 1,710 cm<sup>-1</sup> weaken after KOH doping in the POBP membrane (Supplementary Fig. 12). Moreover, the negative shifts of the N 1s and O 1s spectra of POBP and the appearance of new peaks assigned to N–K and O–K further suggest that there are ion-pair interactions between deprotonated oxindole and K ions (Supplementary Figs. 13 and 14)<sup>29</sup>. In addition to the KOH/oxindole ion pairs, a large amount of free KOH was also absorbed in the membrane, as confirmed by the KOH peaks in the XPS spectra (Supplementary Fig. 13), consistent with the XRD results, which can induce the excellent ion conduction of POBP-ISM in a KOH solution.

POBP membranes also displayed excellent mechanical properties, with a stress of 75.5 MPa and a strain at break of 9.3% (Fig. 2d). More interestingly, the KOH-doped POBP membrane demonstrated negligible stress loss but an increased strain at a break of 31% after KOH doping at a high KOH concentration of 6 M. On increasing the concentration of KOH to 8 M, the tensile strength increased to 63.4 MPa

compared to 58.2 MPa in 6 M, further indicating the increased degree of crystallinity and weakened plasticization of water<sup>30</sup>, which was confirmed by XPS and XRD results. Similar behaviour has also been observed in a PBI-ISM system<sup>30</sup>. Further information on the thermal stability of KOH-doped POBP membranes is given in Supplementary Note 2 (including Supplementary Figs. 15 and 16). Furthermore, the gas permeability is another important property for ISMs used in AWEs, as it determines not only the Faradaic efficiency but also the safety of operation<sup>15,16</sup>. As shown in Fig. 2e, the gas permeability of pristine POBP membranes was 17.8 barrer (1.05 × 10<sup>-15</sup> mol<sup>-1</sup> cm<sup>-1</sup> s<sup>-1</sup> bar<sup>-1</sup>) for H<sub>2</sub> and 1.8 barrer (1.06 × 10<sup>-16</sup> mol<sup>-1</sup> cm<sup>-1</sup> s<sup>-1</sup> bar<sup>-1</sup>) for O<sub>2</sub> at 35 °C (1 barrer = 10<sup>-10</sup> cm<sup>3</sup> (STP) cm cm<sup>-2</sup> s<sup>-1</sup> cmHg<sup>-1</sup>). However, after doping with KOH, the gas permeabilities of the POBP membranes decreased significantly with increasing KOH concentration. The KOH-doped POBP membrane in 6 M KOH showed a H<sub>2</sub> permeability of 6.2 barrer (3.64 × 10<sup>-16</sup> mol<sup>-1</sup> cm<sup>-1</sup> s<sup>-1</sup> bar<sup>-1</sup>) and an O<sub>2</sub> permeability of 0.2 barrer (1.17 × 10<sup>-17</sup> mol<sup>-1</sup> cm<sup>-1</sup> s<sup>-1</sup> bar<sup>-1</sup>). These values are much lower than those of Nafion, the prototypical PEM used in existing commercial PEM water electrolysis, indicating promising applications of AWEs as membranes at elevated operating pressures (Fig. 2e).

### Ionic conductivity

As shown in Fig. 3a, the ion conductivity in the through-plane direction of the POBP membrane was recorded as a function of KOH concentration and temperature. As expected, the ion conductivity of the membrane increased with KOH concentration because there were more sites for ion transportation with a higher-concentration KOH-doped POBP membrane. Moreover, the enhancement of water movement and ion migration induced higher ionic conductivity at elevated temperatures (Fig. 3a). The highest ion conductivity of 86.72 mS cm<sup>-1</sup> was achieved when the POBP membrane was doped with 6 M KOH at 90 °C. Although this value is lower than that of the mPBI membrane because of its lower degree of KOH doping under the same testing conditions, it is high enough for this material to serve as an ISM for AWEs. Upon further increasing the concentration of KOH to 8 M, the ionic conductivity of the POBP membrane decreased, probably due to its lower water uptake, as discussed above.

### Alkaline and oxidative stability

Membrane stabilities, including alkaline and oxidative stabilities, which are crucially important for the practical operation of these membranes in AWEs, were comprehensively evaluated. Impressively, the aryl-ether-free polyaromatics showed robust alkaline stability even under harsh conditions of 8 M KOH at 80 °C. No appreciable change in ionic conductivity (Fig. 3b) was observed even over a long test period of 15,000 h, which is much longer than the stability of PBI-ISMs (refs. 12,15) and previously reported AEMs (ref. 9). Moreover, as shown in Fig. 3d, no detectable change in the chemical shift in the <sup>1</sup>H NMR spectra was observed, further demonstrating the excellent alkaline stability of the polymer backbone and functional groups of oxindole. Furthermore, as shown in Supplementary Fig. 17, there was no obvious change in the chemical shift in the <sup>1</sup>H NMR spectra of POBP before and after the ex situ alkaline stability test (120 °C, 6 M KOH over 300 h), further demonstrating the excellent alkaline stability of the POBP-ISMs even at an elevated temperature of 120 °C. These results were further confirmed by stability testing of model compounds, as discussed above. Therefore, it is remarkable that the POBP-ISMs show competitive alkaline stability and reasonable ion conductivity, which have seldom been achieved simultaneously in previous reports.

The oxidative stability with respect to weight was investigated by immersing membranes in Fenton reagent<sup>31</sup>. As shown in Fig. 3c, the mPBI membrane had poor oxidative stability with a steep weight decline of approximately 35 wt% within 300 h. In contrast, the POBP-ISM exhibited impressive oxidative stability. It remained intact and flexible even after over 1,000 h, with a weight loss of less than 11 wt%. This weight loss

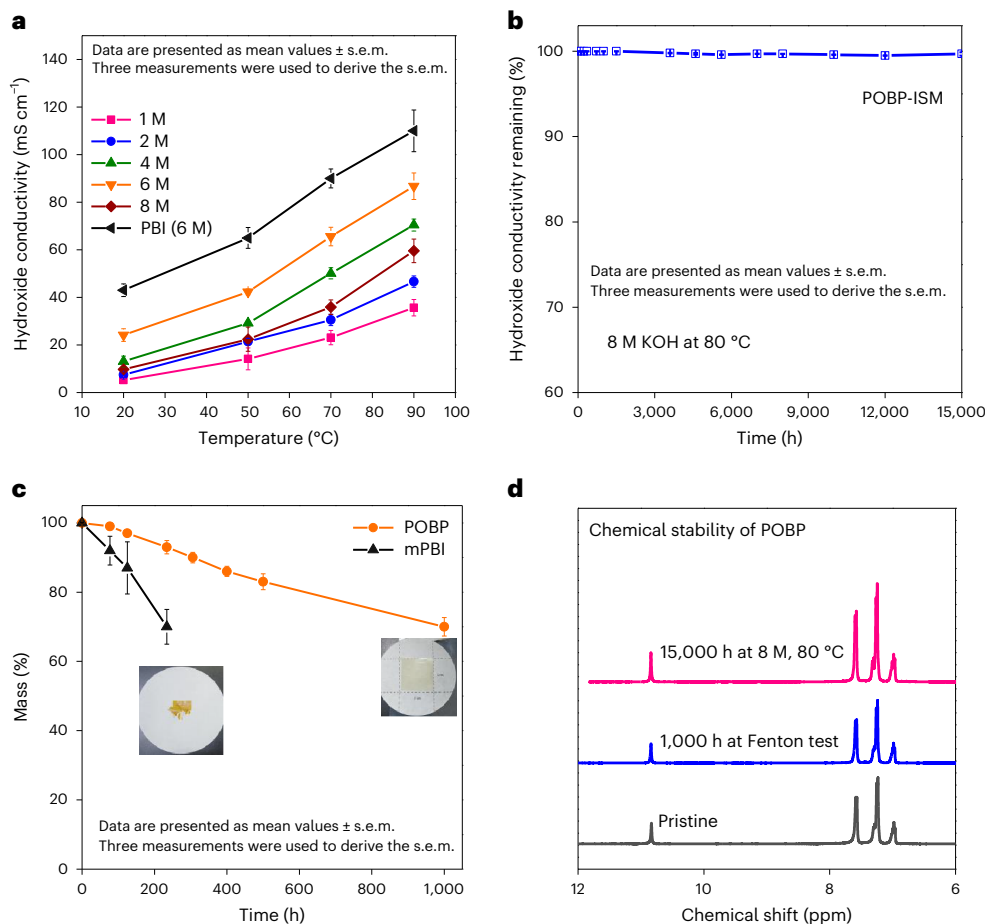


**Fig. 3 | Properties and stability of POBP-ISMs.** **a**, Ion conductivity of membranes as a function of KOH concentration and temperature. **b**, Ion conductivity remaining of membrane during alkaline durability testing (8 M KOH at  $80^{\circ}\text{C}$ ) over 15,000 h. **c**, Comparison of oxidation stability between POBP and mPBI in a Fenton test (4 ppm  $\text{Fe}^{2+}$  at 3 wt%  $\text{H}_2\text{O}_2$  at  $80^{\circ}\text{C}$ ). The insets illustrate the

excellent oxidative stability of the POBP membrane compared to mPBI. **d**,  $^1\text{H}$  NMR spectra of pristine and aged POBP after ex situ alkaline stability testing (15,000 h at 8 M KOH and  $80^{\circ}\text{C}$ ) and Fenton reagent testing (1000 h at  $80^{\circ}\text{C}$ ). Error bars in **a**, **b** and **c** were generated from the standard error of the mean (s.e.m.) derived from three measurements.

of the POBP-ISM was confirmed to be caused by an  $\sim 11\%$  decrease in the thickness, indicating the reasonable surface oxidative degradation of the membrane. More importantly, no obvious changes were observed in the mechanical properties or chemical structures of aged POBP membranes, as confirmed by the Fourier-transform infrared (FT-IR) and NMR spectra (Fig. 3d and Supplementary Figs. 18 and 19). This excellent oxidative stability was attributed to the aryl-ether-free polymer backbone<sup>32</sup> and the lower water uptake of POBP ( $\sim 7$  wt%) in which water was an effective catalyst for radicals to attack the hydrogen-carbon polymer backbone<sup>10,31</sup>.

### AWE device performance and durability

To demonstrate the device performance of POBP-ISMs, an AWE was designed (supplementary Fig. 20) and applied at  $80^{\circ}\text{C}$  in a 6 M aqueous KOH solution using naked Ni foam as a catalyst in both the anode and the cathode due to its high stability despite its low activity. As shown in Fig. 4a, the POBP-ISM exhibited better performance than the state-of-the-art polyphenylene sulfide (PPS) and Zirfon diaphragms. The superior performance of the POBP-ISM was attributed to its relatively low high-frequency resistance (HFR), which was as low as  $\sim 0.203 \Omega \text{ cm}^2$  at  $125 \text{ mA cm}^{-2}$  in 6 M KOH at  $80^{\circ}\text{C}$ . This value is notably lower than for PPS ( $0.402 \Omega \text{ cm}^2$ ) and the Zirfon diaphragm ( $0.287 \Omega \text{ cm}^2$ ). Notably, the thicknesses of PPS ( $700 \pm 10 \mu\text{m}$ ) and Zirfon ( $500 \pm 10 \mu\text{m}$ ) affected their resistance and, thus, the AWE performance. A highly active catalyst is believed to be an effective approach for improving the performance of water electrolysis. As expected

(Fig. 4b), the NiFe-anode-catalysed electrolyser using POBP-ISMs and a Pt/C cathode outperformed the AWEs with a naked Ni foam or Ni/Al alloy catalyst. The optimized electrolyser in 6 M KOH at  $80^{\circ}\text{C}$  had a current density of  $2.0 \text{ A cm}^{-2}$  at 1.9 V, which is comparable to that of the state-of-the-art Nafion 115 in a PEM electrolyser and almost five times higher than that of traditional AWEs based on Ni foam or Ni/Al alloy catalysts ( $\sim 0.4\text{--}0.5 \text{ A cm}^{-2}$  at 1.9 V).

We also investigated the performance of POBP-ISM in various concentrations of KOH (Supplementary Fig. 21). A high KOH concentration induced better performance, probably due to the high ion conductivity (Fig. 3a) and low resistance of the ISMs (Fig. 4c). Thus, because of the remarkable dependence of the ion conductivity and the area resistance on temperature (Fig. 4c), the operating temperature of the electrolyser exerted a substantial influence on the performance of the electrolyser. As shown in Fig. 3a, a high temperature resulted in high conductivity and, thus, better electrolyser performance. Surprisingly, an ISM-based electrolyser easily started at temperatures as low as  $-35^{\circ}\text{C}$  without any external heating system, with a starting time of less than 1 s even after a freezing time of 60 h (Supplementary Figs. 22–24), which is unattainable for PEM or AEM AWEs due to the freezing of pure water. Compared to state-of-the-art porous PPS and Zirfon diaphragms, AWEs based on dense POBP-ISMs showed significant enhancements of 1,700–2,700 times in the transient response times at  $-35^{\circ}\text{C}$  (Supplementary Fig. 25), which is believed to contribute to the lower area resistance of the POBP membrane even at an ultralow temperature of  $-35^{\circ}\text{C}$

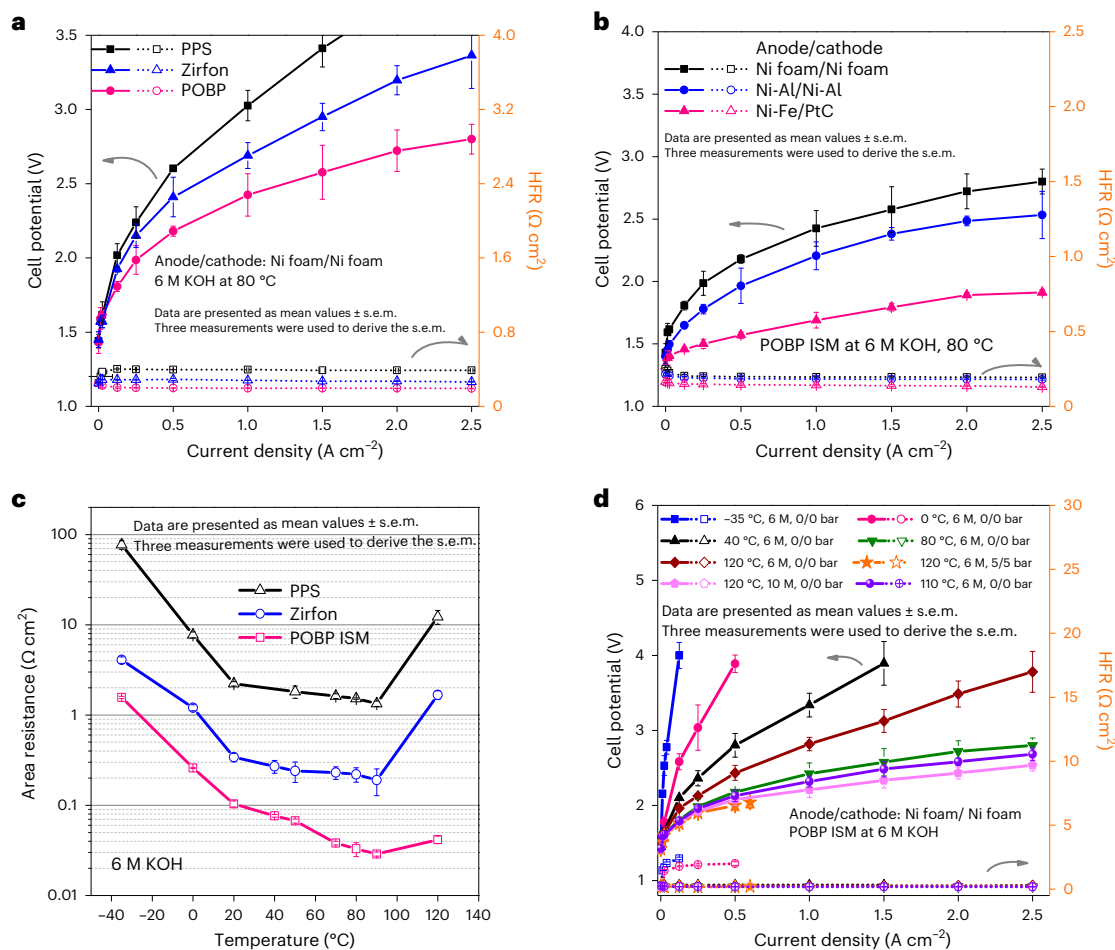


**Fig. 4 | Polarization curves of AWE.** **a**, Comparison of electrolysis polarization and HFR for different membranes: Zirfon (500 ± 10 μm), POBP-ISM (45 ± 5 μm) and PPS diaphragm (700 ± 10 μm). **b**, Electrolysis polarization and HFR for different electrode catalysts with POBP-ISMs at 80 °C. **c**, Comparison of area resistance from -35 to 120 °C of different membranes: Zirfon (500 ± 10 μm),

POBP-ISM (45 ± 5 μm) and PPS diaphragm (700 ± 10 μm). **d**, Polarization characteristics and HFR of electrolysis with POBP-ISMs and Ni-foam catalysts as a function of operating temperature from -35 to 120 °C, electrolyte concentration from 6 to 10 M and pressure from 0 to 5 bar. The error bars were generated from the standard error of the mean (s.e.m.) derived from three measurements.

(Fig. 4c). This result at -35 °C is comparable to that of PBI-ISM, despite the lower conductivity of POBP, due to its lower concentration of ion-pair moieties (Supplementary Fig. 26). This result indicates that the highly alkaline stable POBP-ISM is a promising membrane material for an ISM alkaline electrolyser for fluctuating renewable energy that requires an electrolyser that can be quickly and repeatedly cooled before starting up.

Moreover, as shown in Fig. 4d and Supplementary Fig. 27, improved electrolyser performance and lower HFR were observed at operating temperatures of 110 and 120 °C. When the operating temperature was 120 °C in 6 M KOH at atmospheric pressure, the performance was lower than that of ISMs at 80 °C, probably due to the lower water uptake at temperatures greater than the water boiling point without pressure, which may have increased the area resistance (Fig. 4c). Thus, when the operating temperatures were lower than the boiling point of KOH solution, which was realized by increasing the pressure to 5 bar or the KOH concentration to 10 M, the performance increased and HFR decreased with an increase of temperature (Fig. 4d and Supplementary Fig. 28), indicating the good operability at high temperatures. Like the ultralow-temperature operability, operating PEM and AEM electrolysers at high temperatures of over 80 °C is also unattainable due to the lower  $T_g$  of Nafion and the instability of the AEMs (refs. 6,9), respectively. Therefore, the POBP-ISM alkaline electrolyser has been demonstrated to have one of the broadest operating temperature

ranges achieved thus far for water electrolysis, as it can operate smoothly from -35 to 120 °C.

The high alkaline and oxidative stabilities of the polymer electrolyte membrane are believed to induce high electrolyser device durability. The in situ durability of POBP-ISM was investigated at 80 °C using 6 M KOH alkaline electrolysers with Ni foam as a catalyst. Impressively, the cell voltage remained steady at a voltage as high as 2.3 V for over 2,500 h at 500 mA cm<sup>-2</sup> (Fig. 5a). This superior cell durability was much better than that of mPBI-ISM, for which cell performance obviously decayed after only 130 h under the same testing conditions. The ring-opening degradation mechanism of benzimidazole moieties in mPBI was confirmed by <sup>1</sup>H NMR and FT-IR spectroscopy (Supplementary Figs. 29 and 30). In contrast, after 2,500 h of cell durability testing, the POBP-ISM still showed good solubility and retained its original chemical structure (Supplementary Figs. 31 and 32). No appreciable new peak or chemical shifts of protons were observed in the <sup>1</sup>H NMR and FT-IR spectra, suggesting it has one of the longest periods of stability of alkaline electrolysers under harsh operational environments at a high voltage (~2.3 V), a high temperature (80 °C) and a high KOH concentration (Fig. 5b and Supplementary Fig. 33).

Furthermore, the POBP-ISM AWE had excellent stability at 120 and -35 °C without any obvious decline for 1,000 h (Supplementary Fig. 34). In contrast, the performance of alkaline electrolysers made with Zirfon or mPBI membranes rapidly decreased under the same

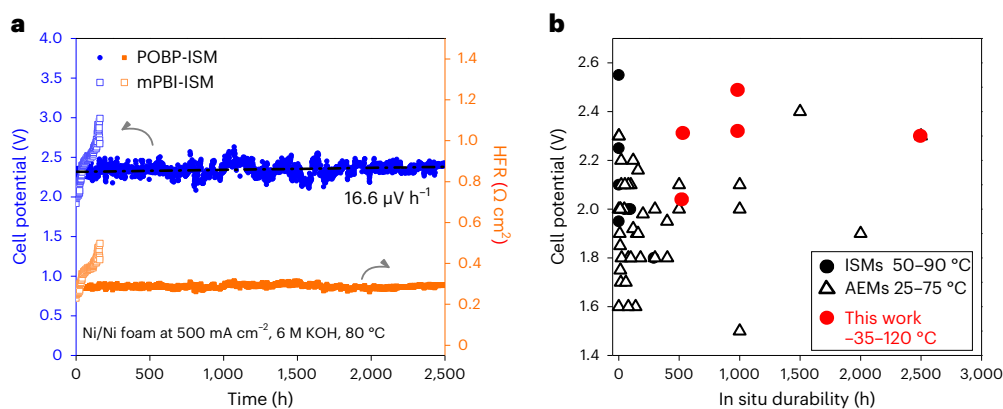


**Fig. 5 | Durability of POBP-ISM AWEs.** **a**, In situ durability of an electrolyser consisting of Ni foam with POBP-ISM at 80 °C. Solid blue circles are the cell voltage durability of POBP-ISM. The solid orange circles are the corresponding HFR of POBP-ISM. The hollow blue squares are the cell voltage durability of mPBI-ISM. The hollow orange squares are the corresponding HFR of mPBI-ISM. **b**, Comparison of in situ durability and cell voltage of present POBP-ISM and current ISMs and AEMs. Red dots denote the present work based on POBP-ISM.

testing conditions. Furthermore, there was a sharp decay in the durability of an electrolyser made with mPBI-ISM at 120 °C in 6 M KOH under 5 bar (Supplementary Fig. 34). Surprisingly, the POBP-ISM could retain its performance for more than 100 h under such the same testing conditions. Although the membrane broke during the durability testing, it was assumed that the high operating pressure resulted in the mechanical failure of the membrane, which was probably due to the unsmooth surface of the Ni foam. Thus, we further tested POBP-ISM in an electrolyser at 120 °C under atmospheric pressure. We increased the KOH concentration to 10 M to increase the boiling point. As expected (Supplementary Fig. 34c), the POBP-ISM could be operated at 120 °C in 10 M KOH and 110 °C in 6 M KOH for more than 500 h. The  $^1\text{H}$  NMR spectrum of POBP after in situ durability testing, as shown in Supplementary Fig. 35, further confirmed its stability. Combined with these high stabilities and durability, particularly at elevated temperatures ( $\geq 80$  °C), the use of a non-precious-metal catalyst, broad operating temperature range, broad KOH concentration range and low gas permeation of the ISM, an operationally flexible AWE with a POBP-ISM was successfully achieved.

## Conclusions

In summary, we established highly stable oxindole/KOH complex ion pairs in POBP-ISMs for AWEs. The high LUMO energy of deprotonated oxindole anions was confirmed by DFT calculations and induced an exciting alkaline stability of the POBP membrane without appreciable conductivity loss over 15,000 h in 8 M KOH at 80 °C. The aryl-ether-free polymer backbone and lower water uptake of the POBP membrane further increased the excellent oxidative stability in a Fenton reagent ( $>1,000$  h at 80 °C). An unoptimized POBP-ISM AWE with a nickel-foam electrode was operated successfully over a broad temperature window ( $-35$  to  $120$  °C) with a rapid start-up ( $<1$  s) even at a low temperature of  $-35$  °C. High performance with an operating current density of  $2.0\text{ A cm}^{-2}$  at  $1.9\text{ V}$  was achieved when an Ni/Fe catalyst was utilized in an anode. This result was comparable with that of an  $\text{IrO}_2$ -anode-catalysed PEM electrolyser. This operational flexibility of POBP-ISM AWE over a wide range of temperatures, a non-precious-metal catalyst, low transient response times and long durability, which is not feasible with existing water electrolysis technology, could enable the simplification and cost reduction of electrolyser systems for green hydrogen production. However, at elevated temperatures of more than  $120$  °C, realizing dimensional, oxidative and polymer backbone alkaline stabilities are still the major challenges in the development of ISMs for AWEs.

Hollow black triangles are for the reported AEMs (refs. 1,6,9,34–48). The solid black circles are ISMs (refs. 13,15,33,49,50). The red dots show the excellent long-term durability (500–2,500 h) and the broad operating temperature range ( $-35$  to  $120$  °C) of our POBP-ISM alkaline electrolysers under present harsh operational environments at a high KOH concentration compared to state-of-the-art ISMs and AEMs.

## Methods

### Materials

Biphenyl (99%), trifluoromethanesulfonic acid (TFSA, 99%), trifluoroacetic acid (TFA, 99%), benzene (99%), 2-phenylbenzimidazole (99%) and isatin (98%) were obtained from Energy Chemical. Dichloromethane (DCM, 99.5%), DMF, DMSO, *N*-methyl-2-pyrrolidone (NMP), *N,N*-dimethylacetamide (DMAc), ethanol (99.7%) and potassium carbonate ( $\text{K}_2\text{CO}_3$ ) were purchased from Sinopharm Chemical Reagent Factory and used as received. Aqueous solutions of KOH with concentrations of 1, 2, 4, 6 and  $8\text{ mol l}^{-1}$  were prepared by dissolving potassium hydroxide pellets (Macklin, GR) in deionized (DI) water.

### Synthesis of 3,3-diphenyloxindole and POBP

3,3-diphenyloxindole was obtained by mixing an excess of benzene (10 ml, 0.113 mol) and isatin (1.66 g, 11.3 mmol) with TFSA (10 equiv.) at 0 °C overnight. To produce high-molecular-weight POBP polymer, isatin (32 g, 21.8 mmol), biphenyl (30 g, 19.4 mmol) and hydrous dichloromethane were typically combined in a 500 ml round-bottom flask. Trifluoroacetic acid (34.0 ml) and TFSA (126.0 ml) were added dropwise at 0 °C. The reaction mixture was agitated at 0 °C for an additional 8 h and then placed into an aqueous ethanol solution and  $1\text{ M K}_2\text{CO}_3$  to remove the residual acid. Finally, with a 99% yield, the white fibrous product was filtered, rinsed with DI water and dried overnight in a vacuum oven at 80 °C. The intrinsic viscosity of POBP was determined to be  $\eta_{\text{int}} = 2.20\text{ dl g}^{-1}$  in DMF at 30 °C. In the  $^1\text{H}$  NMR (400 MHz,  $\text{DMSO-d}_6$ , ppm),  $\delta = 10.85$  (s, 1H), 7.58 (s, 4H), 7.25 (s, 6H) and 6.99 (s, 2H).

### Characterizations of structure

$^1\text{H}$  NMR and  $^{13}\text{C}$  NMR spectroscopy was performed by using a Bruker DPX-400 instrument with  $\text{DMSO-d}_6$  and tetramethylsilane as the solvents and the internal reference, respectively. The FT-IR spectra were recorded on a PerkinElmer Spectrum Two in attenuated total reflectance mode. XPS was performed on a Physical Electronics PHI5600 with an X-ray source operated at 12 kV and 350 W. XRD was carried out using a D8 ADVANCE A25 equipped with a  $\text{Cu K}\alpha$  source ( $\lambda = 1.54184\text{ \AA}$ ) in the range  $5$ – $50^\circ 2\theta$  at a scan speed of  $4^\circ/2\theta$  per minute and a step size of  $0.02^\circ/2\theta$ . The  $d$  spacing for the amorphous or crystalline peak maxima was calculated according to the Bragg equation.

### Membrane preparation

The solution (filtered 8 wt% POBP in DMF) was cast in a clean glass dish at 80 °C for at least 24 h in an oven. After immersing the glass in DI

water, the membrane was pulled off and left until it disengaged from the glass. POBP-ISMs were obtained by immersing the membrane in aqueous KOH with concentrations ranging from 0 to 8 M at 80 °C for at least a week. The thickness of the obtained membrane was  $45 \pm 5 \mu\text{m}$ .

### Characterization of the POBP-ISMs

The hydrophilicity of the membranes after doping in different aqueous KOH concentrations ranging from 0 to 8 M was determined from the contact angle, using DI water on the surface of the membranes. The KOH content and water content of the ISMs were determined gravimetrically using the method described by previous works<sup>13,16</sup>. The weight fractions of POBP ( $W_p$ ), water ( $W_w$ ) and KOH equivalents ( $W_{\text{KOH}}$ ) were calculated as follows:

$$W_p = \frac{m_{\text{dedoped}}}{m} \times 100\%, \quad (1)$$

$$W_w = \frac{(m - m_{\text{dry}})}{m} \times 100\%, \quad (2)$$

$$W_{\text{KOH}} = \frac{(m_{\text{dry}} - m_{\text{dedoped}})}{m} \times 100\%, \quad (3)$$

where  $m$  is the weight of a membrane sample after being carefully wiped with tissue paper,  $m_{\text{dry}}$  is the weight of a sample after drying at 120 °C for 12 h in a vacuum and  $m_{\text{dedoped}}$  is the weight of a sample of membrane after extensive washing in DI water until neutral pH followed by drying at 120 °C for 12 h. The swelling ratios (SRs) in the surface area ( $\text{SR}_A$ ) and thickness ( $\text{SR}_T$ ) of the membranes were recorded to determine the swelling characteristics of a dried membrane. The SRs of the membranes were calculated as follows:

$$\text{SR}_T = \frac{T_{\text{wet}} - T_{\text{dry}}}{T_{\text{dry}}} \times 100\%, \quad (4)$$

$$\text{SR}_A = \frac{A_{\text{wet}} - A_{\text{dry}}}{A_{\text{dry}}} \times 100\%, \quad (5)$$

where  $T_{\text{dry}}$  and  $A_{\text{dry}}$  are the thickness and surface area of a dried membrane before doping and  $T_{\text{wet}}$  and  $A_{\text{wet}}$  are the thickness and surface area of a hydrated membrane, respectively. The pure gas permeation properties of membranes were evaluated by a constant-volume/variable-pressure method (constant downstream volume permeation apparatus). Before testing, each membrane was degassed for 24 h. Three different samples of the membranes equilibrated in aqueous bulk KOH solution were tested, and the deviation was less than 5%. The permeability was calculated as follows:

$$P = 10^{10} \times \frac{V_d l}{P_{\text{up}} T R A} \times \frac{dp}{dt}, \quad (6)$$

where  $P$  is the permeability (barrer) and 1 barrer =  $10^{-10} \text{ cm}^3 \text{ (STP) cm cm}^{-2} \text{ s}^{-1} \text{ cmHg}^{-1}$ .  $V_d$  is the calibrated permeate volume ( $\text{cm}^3$ ),  $l$  is the membrane thickness (cm),  $P_{\text{up}}$  is the upstream pressure (cmHg),  $A$  is the effective membrane area ( $\text{cm}^2$ ),  $T$  is the operating temperature (K),  $R$  is the gas constant ( $0.278 \text{ cm}^3 \text{ cmHg cm}^{-3} \text{ (STP) K}^{-1}$ ) and  $dp/dt$  is the rate of change of the steady-state downstream pressure ( $\text{cmHg s}^{-1}$ ). The storage modulus and  $\tan \delta$  of POBP membranes were measured by a dynamic thermomechanical analysis system (Q800, TA Instruments). Membrane samples were cut into 9 mm × 40 mm rectangles and then measured with a preload force of 0.01 N and a force track of 125% under  $\text{N}_2$  atmosphere. The sample was ramped at  $4 \text{ }^\circ\text{C min}^{-1}$  until 460 °C. The peak of  $\tan \delta$  represents the glass transition temperature ( $T_g$ ) of a membrane sample. The mechanical properties of a membrane

were measured using a mechanical testing instrument (CMT-4502, MTS Systems Co.) at a crosshead speed of  $5 \text{ mm min}^{-1}$  at 40% relative humidity. The thermal stability of doped membranes was investigated by thermogravimetric analysis using a PerkinElmer TGA-7 thermogravimetric analyser at a heating rate of  $10 \text{ }^\circ\text{C min}^{-1}$  under a nitrogen atmosphere. All membranes were dried in a vacuum oven at 110 °C overnight before analysis.

### Computational details and simulations

The alkaline stability was assessed as follows. Theoretical calculations of 3,3-diphenyloxindole and 2-phenylbenzimidazole salt molecules were performed by Dmol embedded in the Materials Studio software system package<sup>23</sup>. The GGA-BLYP functional and double numerical plus polarization basis set were used for the calculations. The single molecules were all optimized with a self-consistent field convergence value of  $10^{-6}$  Ha. Considering the solution surroundings, the impact of the solvent (water,  $\epsilon = 78.54$ ) was incorporated into the calculations.

### Conductivity measurement

The through-plane conductivity of POBP after alkaline equilibration by immersion in aqueous KOH was obtained using impedance spectroscopy with an impedance/gain phase analyser (Bio-Logic VSP-300) over the frequency range from 50 mHz to 100 kHz according to previous reports<sup>13,15,33</sup>. Separate samples had an active area of  $2.0 \text{ cm}^2$  and were mounted between two chambers of a H cell with a Pt electrode. The interspace was filled with the corresponding KOH solution. The conductivity was calculated as follows:

$$\sigma = \frac{t}{A \times (R - R_{\text{blank}})}. \quad (7)$$

The area resistance was calculated as follows:

$$\text{AR} = A \times (R - R_{\text{blank}}) \quad (8)$$

where  $t$  (cm) is the thickness of the membrane,  $R$  ( $\Omega$ ) is the resistance of the electrodes with the membrane,  $R_{\text{blank}}$  ( $\Omega$ ) is the resistance of the electrodes without the membrane and  $A$  ( $\text{cm}^2$ ) represents the available cross-sectional membrane area.

### Chemical stability

The alkaline stability was assessed as follows. The POBP was evaluated in 8 M KOH at 80 °C and 6 M KOH at 120 °C, and the variations in the membranes before and after the alkaline stability test were also analysed by FT-IR spectroscopy,  $^1\text{H NMR}$  and conductivity measurements. The oxidative stability was assessed as follows. A Fenton test (4 ppm  $\text{Fe}^{2+}$  in 3 wt%  $\text{H}_2\text{O}_2$  at 80 °C) was used to detect the weight loss and chemical changes in membranes caused by radical-induced oxidation. After a certain period, the membranes were removed, thoroughly washed with DI water and dried at 120 °C for 8 h before testing. To continue the test, the membrane samples were placed in newly produced Fenton solutions.

### Performance and durability for AWE

The AWE experiments were carried out using our homemade electrolyzers<sup>6,16</sup>. An optimized membrane electrode assembly (MEA) was prepared as follows. A catalyst-coated membrane was used to fabricate the MEA using Fe-Ni as the anode and Pt/C as the cathode. Typically, the anode catalyst was a suspension of a catalyst, isopropanol, DI water and an ionomer (FAA-3). The catalyst link of the cathode was a suspension of Pt/C, isopropanol, DI water and the ionomer. An unoptimized MEA was prepared as follows. A catalyst-coated substrate was used to fabricate the MEA using nickel foam or Ni-Al electrodes as the anode and cathode. The electrolysis cell consisted of flow-field plates with a linear pattern made from nickel, electrodes ( $9 \text{ cm}^2$ ), a membrane ( $4 \text{ cm}^2$ ) and gaskets ( $25 \text{ cm}^2$ ). Heating elements and a thermocouple were placed within the flow-field



plates to control the temperature. A CT-4008-5V10A-FA instrument (NEWARE) controlled by a cell testing system was used for the power supply. The KOH electrolyte was actively circulated through the electrodes at 60 ml min<sup>-1</sup>. The electrolyser was conditioned at 10 mA cm<sup>-2</sup> for 40–60 min to reach a steady state. The polarization curves for the MEA were measured in galvanostatic mode at 10–2,500 mA cm<sup>-2</sup> from –35 to 120 °C under atmospheric or predetermined pressure. The transient response times were found from *I*–*V* curves, which were recorded after 0, 15, 40 and 60 h of operation by scanning the current density at –35 °C. The transient response time of the AWE was determined from the cell potential over the theoretical electrolytic potential. Gas was generated at the anode and cathode poles. Electrochemical impedance spectroscopy was performed in constant current density mode on a multichannel electrochemical station (Ivium). The frequency was in the range 10<sup>5</sup> to 0.1 Hz, and the amplitude was 100 mA.

The durability of the AWE as assessed as follows. The aforementioned approach using nickel-foam electrodes was utilized to assess the in situ durability of the ISMs. The electrolyser was set to 500 mA cm<sup>-2</sup> with 6 M KOH at –35, 80, 110 or 120 °C, 10 M KOH at 120 °C under atmospheric pressure and 6 M KOH at 120 °C under 5 bar. The water and electrolyte were supplied manually, generally after approximately 12 h.

## Data availability

The authors declare that the data supporting the findings of this study are available within the paper, Supplementary Information and Source Data files. Further data beyond the immediate results presented here are available from the corresponding authors upon reasonable request. Source data are provided with this paper.

## References

- Li, D. et al. Highly quaternized polystyrene ionomers for high performance anion exchange membrane water electrolyzers. *Nat. Energy* **5**, 378–385 (2020).
- Abbasi, R. et al. A roadmap to low-cost hydrogen with hydroxide exchange membrane electrolyzers. *Adv. Mater.* **31**, e1805876 (2019).
- Schug, C. A. Operational characteristics of high-pressure, high-efficiency water-hydrogen-electrolysis. *Int. J. Hydrogen Energy* **23**, 1113–1120 (1998).
- Lohmann-Richters, F. P., Renz, S., Lehnert, W., Müller, M. & Carmo, M. Review—challenges and opportunities for increased current density in alkaline electrolysis by increasing the operating temperature. *J. Electrochem. Soc.* **168**, 114501 (2021).
- Lee, B., Lim, D., Lee, H. & Lim, H. Which water electrolysis technology is appropriate? Critical insights of potential water electrolysis for green ammonia production. *Renew. Sustain. Energy Rev.* **143**, 110963 (2021).
- Hu, X. et al. Piperidinium functionalized aryl ether-free polyaromatics as anion exchange membrane for water electrolyzers: performance and durability. *J. Membr. Sci.* **621**, 118964 (2021).
- Jiao, K. et al. Designing the next generation of proton-exchange membrane fuel cells. *Nature* **595**, 361–369 (2021).
- Olsson, J. S., Pham, T. H. & Jannasch, P. Poly(arylene piperidinium) hydroxide ion exchange membranes: synthesis, alkaline stability, and conductivity. *Adv. Funct. Mater.* **28**, 1702758 (2018).
- Li, D. et al. Durability of anion exchange membrane water electrolyzers. *Energy Environ. Sci.* **14**, 3393 (2021).
- Holmes, T., Skalski, T. J. G., Adamski, M. & Holdcroft, S. Stability of hydrocarbon fuel cell membranes: reaction of hydroxyl radicals with sulfonated phenylated polyphenylenes. *Chem. Mater.* **31**, 1441–1449 (2019).
- Tang, H. et al. Fuel cells with an operational range of –20 °C to 200 °C enabled by phosphoric acid-doped intrinsically ultramicroporous membranes. *Nat. Energy* **7**, 153–162 (2022).
- Kraglund, M. R. et al. Ion-solvating membranes as a new approach towards high rate alkaline electrolyzers. *Energy Environ. Sci.* **12**, 3313–3318 (2019).
- Aili, D. et al. Towards a stable ion-solvating polymer electrolyte for advanced alkaline water electrolysis. *J. Mater. Chem. A* **5**, 5055–5066 (2017).
- Xing, B. & Savadogo, O. Hydrogen/oxygen polymer electrolyte membrane fuel cells (PEMFCs) based on alkaline-doped polybenzimidazole (PBI). *Electrochem. Commun.* **2**, 697–702 (2000).
- Hu, B. et al. A stable ion-solvating PBI electrolyte enabled by sterically bulky naphthalene for alkaline water electrolysis. *J. Membr. Sci.* **643**, 120042 (2022).
- Hu, X., Liu, M., Huang, Y., Liu, L. & Li, N. Sulfonate-functionalized polybenzimidazole as ion-solvating membrane toward high-performance alkaline water electrolysis. *J. Membr. Sci.* **663**, 121005 (2022).
- Grigoriev, S. A., Fateev, V. N., Bessarabov, D. G. & Millet, P. Current status, research trends, and challenges in water electrolysis science and technology. *Int. J. Hydrogen Energy* **45**, 26036–26058 (2020).
- Zhang, K. et al. Status and perspectives of key materials for PEM electrolyzer. *Nano Res. Energy* **1**, e9120032 (2022).
- Hernandez, M. C. G. et al. Novel, metal-free, superacid-catalyzed ‘click’ reactions of isatins with linear, nonactivated, multiring aromatic hydrocarbons. *Macromolecules* **43**, 6968–6979 (2010).
- Hossain, I., Husna, A., Jeong, I. & Kim, T.-H. Biphenyl(isatin-*n*-co-trifluoroacetophenone)-based copolymers synthesized using the Friedel–Crafts reaction as mechanically robust membranes for efficient CO<sub>2</sub> separation. *ACS Appl. Polym. Mater.* **4**, 3779–3790 (2022).
- Zhang, S., Zhu, X. & Jin, C. Development of a high-performance anion exchange membrane using poly(isatin biphenylene) with flexible heterocyclic quaternary ammonium cations for alkaline fuel cells. *J. Mater. Chem. A* **7**, 6883–6893 (2019).
- Pulido, B., Chisca, S. & Nunes, S. P. Solvent and thermal resistant ultrafiltration membranes from alkyne-functionalized high-performance polymers. *J. Membr. Sci.* **564**, 361–371 (2018).
- Lin, B. et al. Alkaline stable C2-substituted imidazolium-based anion-exchange membranes. *Chem. Mater.* **25**, 1858–1867 (2013).
- Klumpp, D. A., Yeung, K. Y., Surya Prakash, G. K. & Olah, G. A. Preparation of 3,3-diaryloxindoles by superacid-induced condensations of isatins and aromatics with a combinatorial approach. *J. Org. Chem.* **63**, 4 (1998).
- Cruz, A. R. et al. Precision synthesis of narrow polydispersity, ultrahigh molecular weight linear aromatic polymers by A2 + B2 nonstoichiometric step-selective polymerization. *Macromolecules* **45**, 6774–6780 (2012).
- Bruce, J. M. & Sutcliffe, F. K. Heterocyclic compounds of nitrogen. Part I. The alkylation and acylation of 3-phenyloxindole, and the preparation of some derivatives of 2-hydroxy-3-phenylindole. *J. Chem. Soc.* **1957**, 4789–4798 (1957).
- Bordwell, F. G. & Fried, H. E. Heterocyclic aromatic anions with 4n+2 π-electrons. *J. Org. Chem.* **56**, 4218–4224 (1991).
- Wang, J. W., Jiang, L., Huang, H. H., Han, Z. & Ouyang, G. Rapid electron transfer via dynamic coordinative interaction boosts quantum efficiency for photocatalytic CO<sub>2</sub> reduction. *Nat. Commun.* **12**, 4276 (2021).
- Zeng, L., Zhao, T. S., An, L., Zhao, G. & Yan, X. H. Physicochemical properties of alkaline doped polybenzimidazole membranes for anion exchange membrane fuel cells. *J. Membr. Sci.* **493**, 340–348 (2015).
- Aili, D. et al. Understanding ternary poly(potassium benzimidazolide)-based polymer electrolytes. *Polymer* **84**, 304–310 (2016).

31. Chang, Z. et al. Chemical oxidative degradation of polybenzimidazole in simulated environment of fuel cells. *Polym. Degrad. Stab.* **94**, 1206–1212 (2009).
32. Wang, J. et al. Poly(aryl piperidinium) membranes and ionomers for hydroxide exchange membrane fuel cells. *Nat. Energy* **4**, 392–398 (2019).
33. Kraglund, M. R. et al. Zero-gap alkaline water electrolysis using ion-solvating polymer electrolyte membranes at reduced KOH concentrations. *J. Electrochem. Soc.* **163**, F3125–F3131 (2016).
34. Choe, Y.-K. et al. Alkaline stability of benzyl trimethyl ammonium functionalized polyaromatics: a computational and experimental study. *Chem. Mater.* **26**, 5675–5682 (2014).
35. Vengatesan, S., Santhi, S., Jeevanantham, S. & Sozhan, G. Quaternized poly(styrene-co-vinylbenzyl chloride) anion exchange membranes for alkaline water electrolyzers. *J. Power Sources* **284**, 361–368 (2015).
36. Liu, Z. et al. The effect of membrane on an alkaline water electrolyzer. *Int. J. Hydrogen Energy* **42**, 29661–29665 (2017).
37. Chu, X., Shi, Y., Liu, L., Huang, Y. & Li, N. Piperidinium-functionalized anion exchange membranes and their application in alkaline fuel cells and water electrolysis. *J. Mater. Chem. A* **7**, 7717–7727 (2019).
38. Li, D. et al. Phenyl oxidation impacts the durability of alkaline membrane water electrolyzer. *ACS Appl. Mater. Interfaces* **11**, 9696–9701 (2019).
39. Li, H. et al. Poly(vinyl benzyl methylpyrrolidinium) hydroxide derived anion exchange membranes for water electrolysis. *J. Mater. Chem. A* **7**, 17914–17922 (2019).
40. Su, X. et al. Novel piperidinium functionalized anionic membrane for alkaline polymer electrolysis with excellent electrochemical properties. *J. Membr. Sci.* **581**, 283–292 (2019).
41. Cha, M. S. et al. Poly(carbazole)-based anion-conducting materials with high performance and durability for energy conversion devices. *Energy Environ. Sci.* **13**, 3633–3645 (2020).
42. Lee, H. I. et al. Advanced Zirfon-type porous separator for a high-rate alkaline electrolyser operating in a dynamic mode. *J. Membr. Sci.* **616**, 118541 (2020).
43. Park, H. J., Lee, S. Y., Lee, T. K., Kim, H.-J. & Lee, Y. M. N3-butyl imidazolium-based anion exchange membranes blended with poly(vinyl alcohol) for alkaline water electrolysis. *J. Membr. Sci.* **611**, 118355 (2020).
44. Park, Y. S. et al. Superior performance of anion exchange membrane water electrolyzer: ensemble of producing oxygen vacancies and controlling mass transfer resistance. *Appl. Catal. B* **278**, 119276 (2020).
45. Yan, X. et al. Twisted ether-free polymer based alkaline membrane for high-performance water electrolysis. *J. Power Sources* **480**, 228805 (2020).
46. Chen, N. et al. High-performance anion exchange membrane water electrolyzers with a current density of 7.68 Acm<sup>-2</sup> and durability of 1000 h. *Energy Environ. Sci.* **14**, 6338–6348 (2021).
47. Xu, Z. et al. Anisotropic anion exchange membranes with extremely high water uptake for water electrolysis and fuel cell. *J. Mater. Chem. A* **9**, 23485 (2021).
48. Liu, M., Hu, X., Hu, B., Liu, L. & Li, N. Soluble poly(aryl piperidinium) with extended aromatic segments as anion exchange membranes for alkaline fuel cells and water electrolysis. *J. Membr. Sci.* **642**, 119966 (2022).
49. Diaz, L. A. et al. Alkali-doped polyvinyl alcohol – polybenzimidazole membranes for alkaline water electrolysis. *J. Membr. Sci.* **535**, 45–55 (2017).
50. Konovalova, A. et al. Blend membranes of polybenzimidazole and an anion exchange ionomer (FAA3) for alkaline water electrolysis: improved alkaline stability and conductivity. *J. Membr. Sci.* **564**, 653–662 (2018).

## Acknowledgements

We thank X. Zhang from Nanjing University of Science and Technology for the simulations and M. Dou at the Institute of Coal Chemistry of the Chinese Academy of Sciences for help with the NMR. We also thank Shiyanjia Lab ([www.shiyanjia.com](http://www.shiyanjia.com)) for support during the DFT test. Financial support for this work was provided by the National Natural Science Foundation of China (Grant Nos. 21835005 and 22105217), the STS Project of the Chinese Academy of Sciences (Grant No. KFJ-ST-S-QYZD-2021-02-003) and the Natural Science Foundation of Shanxi Province (Grant No. 20210302124433).

## Author contributions

N.L. initiated this collaborative project. K.G. helped with data collection and the formal analysis. X.H. synthesized the polymeric materials, designed the experiments and wrote the original draft of the manuscript. C.N. and J.Y. set up the testing system at high operating pressure and high temperature and collected the data. K.G., B.H., M.L., H.T. and S.K. characterized the electrolyser tests and reviewed the draft of the manuscript. Y.H., N.L. and K.G. contributed to the writing of the manuscript. K.G. and N.L. supervised and guided the work.

## Competing interests

The authors declare no competing interests.

## Additional information

**Supplementary information** The online version contains supplementary material available at <https://doi.org/10.1038/s41560-023-01447-w>.

**Correspondence and requests for materials** should be addressed to Kang Geng or Nanwen Li.

**Peer review information** *Nature Energy* thanks Patric Jannasch, Jens Oluf Jensen and Yu Seung Kim for their contribution to the peer review of this work.

**Reprints and permissions information** is available at [www.nature.com/reprints](http://www.nature.com/reprints).

**Publisher's note** Springer Nature remains neutral with regard to jurisdictional claims in published maps and institutional affiliations.

Springer Nature or its licensor (e.g. a society or other partner) holds exclusive rights to this article under a publishing agreement with the author(s) or other rightsholder(s); author self-archiving of the accepted manuscript version of this article is solely governed by the terms of such publishing agreement and applicable law.

© The Author(s), under exclusive licence to Springer Nature Limited 2024